Exploiting Close-to-the-Sensor Multipath Reflections Using a Human-Hearing-Inspired Model

Satyabrata Sen and Arye Nehorai

***Abstract*—We propose a simple three-dimensional (3-D) direction-finding system that exploits multipath reflections close to the sensors to improve performance by increasing the effective array aperture. Such close-range multipath reflections can originate, for example, from parts of the platform on which the sensor is mounted. Our system is inspired by the human auditory system where multipath reflections from the external ear (pinna) enable 3-D direction finding. To demonstrate the advantage of exploiting multipath reflections, we consider a simple example of a passive system with only one sensor and two nearby reflectors. First, we present a parametric measurement model and then compute the asymptotic Cramér–Rao bound on the 3-D direction estimates for a stochastic source signal of unknown parametrized spectrum. We provide a few numerical examples to illustrate our analytical results. We find that for this example additional reflectors and a wider source spectrum can achieve better direction estimates.**

***Index Terms*—Biologically inspired, human hearing analysis, multipath exploitation, 3-D direction finding.**

I. Introduction

Direction estimation of a target is one of the major problems in radar, sonar, navigation, and robotics. Over the past few decades, a wide variety of techniques have been proposed to solve these problems using sensor arrays. Since the estimation accuracy improves with an increasing number of sensors, many systems use a large number of sensors in different configurations. However, due to a variety of tactical problems, it is not always possible to use a large sensor array. In any practical system there are reflections from parts of the platform or vehicle on which the sensor is mounted. For example, in a ground radar, multipath signals occur due to reflections from different body parts of the vehicle. Conventional systems try to suppress these multipath reflections by treating them as interference. In this correspondence we demonstrate that by exploiting known close-range reflections we can improve the target-direction estimation.

A. Motivation

Our system is inspired by the human auditory system, which performs remarkably well in finding the direction of sound sources in 3-D with just two ears. This performance is possible because of the anatomy of the external ears (pinnae) [1]. When the wavelength is of the same order or shorter than the dimension of the ear, different ridges and notches of the external ear interact significantly with the incident sound, as shown in Fig. 1. Batteau suggested two major ridges in the external ear that act like reflecting surfaces, producing close-range multipath echoes that yield important cues for direction estimation.

Manuscript received June 30, 2008; revised September 28, 2008. First published October 31, 2008; current version published January 30, 2009. This work was supported in part by DARPA by Grant HR0011-07-1-0036, by the Department of Defense under the Air Force Office of Scientific Research MURI Grant FA9550-05-1-0443, and by the ONR by Grant N000140810849. The associate editor coordinating the review of this manuscript and approving it for publication was Prof. Andreas Jakobsson.

The authors are with the Department of Electrical and Systems Engineering Washington University, St. Louis, MO 63130 USA (e-mail: ssen3@ese.wustl.edu; nehorai@ese.wustl.edu).

Color versions of one or more of the figures in this correspondence are available online at http://ieeexplore.ieee.org.

Digital Object Identifier 10.1109/TSP.2008.2008257

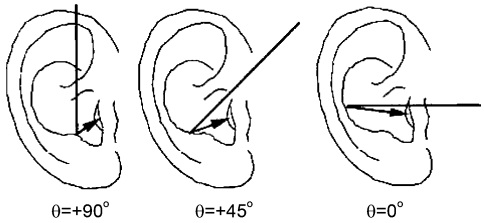

Fig. 1. Pinna reflections of sound from different directions of arrival [11].

Over the years, researchers have tried to find experimental evidence that pinna reflections are the major cues for finding elevation angle [2]–[4]. Today, it is well established that, in addition to the pinnae, the human torso, shoulders, and head diffract the incoming sound waves. Collectively, these propagation effects are termed the head-related transfer function (HRTF). Brown and Duda provided some empirical formulae for the multipath delays produced by the pinna [5]. Harris *et al.* [6] built a VLSI circuitry of 2-D sound localization system inspired by HRTF models. However, they did not include any performance analysis of their system. In [7] we presented statistical performance analysis of the Brown-Duda HRTF model for 3-D direction finding.

B. Outline

In this correspondence, we model and analyze a 3-D direction-finding system that exploits multipath reflections close to the sensor. To demonstrate our approach, we present a parametric measurement model of a passive system with only one sensor and two nearby reflectors in Section II. Our system can be generalized to a more complicated system having multiple reflectors at known positions with respect to the sensor. We analyze the performance of this system for a zero-mean wide-sense stationary Gaussian source signal by computing the asymptotic frequency domain Cramér–Rao bound (CRB) on the error of the 3-D direction estimate in Section III. We model the spectrum of the source signal in terms of a few unknown parameters. Our numerical examples, presented in Section IV, illustrate the ability of our model to estimate the directional angles and the parameters of the source spectrum in various scenarios. Section V contains the conclusions and highlights a few possible directions for future work.

II. Measurement Model

In this section, we propose a measurement model for exploiting multipath propagation effects due to nearby reflectors. We consider a simple 3-D model as shown in Fig. 2. We choose a Cartesian coordinate system such that the sensor is located at the origin. There are two reflectors close to the sensor: one is parallel to the XY plane at a distance $z_{\rm r}$ from the sensor, and the other is parallel to the XZ plane at a distance $y_{\rm r}$ from the sensor. We consider a static far-field point target, located at $(x_{\rm t}, y_{\rm t}, z_{\rm t})$ where $y_{\rm t} > 0$ and $z_{\rm t} > 0$. In reference to a standard spherical coordinate system the elevation angle (θ) and the azimuth angle (ϕ) of the target can be expressed as $\theta = \cos^{-1}(z_{\rm t}/r)$ and $\phi = \cos^{-1}(x_{\rm t}/r \sin\theta)$, respectively, where $r = \sqrt{x_{\rm t}^2 + y_{\rm t}^2 + z_{\rm t}^2}$. From Fig. 2 it is evident that if the reflectors were not present, it would not be possible to estimate the directions of the target. Furthermore, if only the reflector parallel to the XY plane were present then only the elevation angle could be estimated. Here, we want to show that the multipath reflections produced by these two nearby reflectors enable the estimation of both elevation and azimuth angles.

We assume that at the operating frequency the reflecting surfaces behave as smooth flat surfaces, producing only specular reflections. The

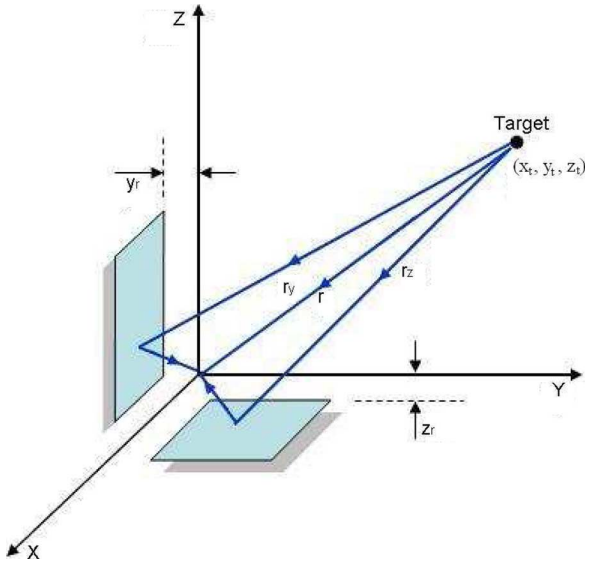

Fig. 2. Multipath reflections close to the sensor.

reflection points on the surfaces can be located by applying Snell's law of reflection: the angle of reflection is equal to the angle of incidence. In our problem of interest, one specular reflection point exists on each reflector. Considering only first-order reflections, the total received signal $y(t)$ can be modeled as a coherent sum of three signals

$$y(t) = s(t) + \rho_z s(t-\tau_z) + \rho_y s(t-\tau_y) + e(t) \tag{1}$$

where $s(t)$ is the direct signal, ρ_z and ρ_y are the reflection coefficients of the reflectors, and $e(t)$ is the measurement noise. Here τ_z and τ_y denote the time delays between the direct path and the reflected paths due to the reflectors parallel to the XY plane and XZ plane, respectively. Assuming $z_{\rm r} \ll r$ we can deduce τ_z as follows:

$$\begin{aligned}\tau_z &= \frac{r_z - r}{c} = \frac{\sqrt{x_{\rm t}^2 + y_{\rm t}^2 + (z_{\rm t}+2z_{\rm r})^2} - r}{c} \\ &= \frac{r}{c}\left[\sqrt{1 + \frac{4z_{\rm r}\cos\theta}{r} + \frac{4z_{\rm r}^2}{r^2}} - 1\right] \\ &\approx \frac{r}{c}\left[\sqrt{1 + \frac{4z_{\rm r}\cos\theta}{r}} - 1\right] \\ &\approx \frac{r}{c}\left[\left(1 + \frac{1}{2}\cdot\frac{4z_{\rm r}\cos\theta}{r}\right) - 1\right] = \frac{2z_{\rm r}}{c}\cos\theta. \end{aligned} \tag{2}$$

Similarly, assuming $y_{\rm r} \ll r$ we can evaluate τ_y as

$$\tau_y = \frac{2y_{\rm r}}{c}\sin\theta\sin\phi. \tag{3}$$

Assuming that the positions of the reflectors ($z_{\rm r}$ and $y_{\rm r}$) are known to the receiver, the elevation and azimuth angles (θ, ϕ) can be estimated from the estimates of τ_z and τ_y using (2), (3). Denoting $h(t) = 1 + \rho_z\delta(t-\tau_z) + \rho_y\delta(t-\tau_y)$ as the impulse response of the channel between the target and the sensor, (1) can be written as $y(t) = h(t) * s(t) + e(t)$, where $*$ denotes the convolution operator. The corresponding frequency response of the channel filter is

$$H(\omega) = 1 + \rho_z e^{-j\omega\tau_z} + \rho_y e^{-j\omega\tau_y}. \tag{4}$$

III. Performance Measure

In this section, we compute the Cramér–Rao bound (CRB) on the errors of the direction estimates (θ, ϕ). We begin by stating a few statistical assumptions of our model.

A. Statistical Assumptions

We assume that both the source signal and noise are zero-mean wide-sense stationary processes, uncorrelated with each other. Therefore, the power spectral density $S_y(\omega)$ of the received signal $y(t)$ can be expressed as

$$S_y(\omega) = |H(\omega,\theta,\phi)|^2 S_s(\omega,\mathbf{a}) + S_e(\omega) \tag{5}$$

where $S_s(\omega,\mathbf{a})$ and $S_e(\omega)$ are the power spectral densities of the source signal $s(t)$ and the measurement noise process $e(t)$, respectively. We parametrize the source spectrum in terms of n unknowns $\mathbf{a} = [\,a_1 \quad a_2 \quad \cdots \quad a_n\,]^T$. For example, in Section IV we consider an example with a second-order autoregressive (AR) process whose power spectral density is modeled in terms of two unknown coefficients a_1 and a_2. Furthermore, for simplicity we assume that the power spectral density of the noise process is flat; i.e., $S_e(\omega) = S_e$.

B. Cramér–Rao Bound

The CRB is a universal lower bound on the variance of all unbiased estimators of a set of parameters. It is defined as the inverse of the Fisher information matrix (FIM), which describes the amount of information about the unknown parameters provided by the measured data. Let $y(t) = [\,y(1) \quad y(2) \quad \ldots \quad y(N)\,]^T$ be a measurement vector that is a function of an unknown M-element parameter vector ψ, and let $\hat{\psi}$ be an unbiased estimate of ψ. Under mild regularity assumptions, $\mathbf{CRB}(\hat{\boldsymbol{\psi}}) \geq \mathbf{J}^{-1}(\boldsymbol{\psi})$, where $\mathbf{J}(\boldsymbol{\psi})$ denotes the FIM. When $\mathbf{y}(t)$ is a zero-mean wide-sense stationary Gaussian process, a convenient formula for computing the asymptotic form (i.e., large N) of the FIM was given by Whittle [8]: see (6) at the bottom of the page, where $\mathbf{S}_y(\omega,\boldsymbol{\psi})$ denotes the power-spectral density matrix of $\mathbf{y}(t)$; see [9, Ch. 3], [10] for details.

To apply Whittle's formula to our model, we assume that both the source signal and noise are zero-mean wide-sense stationary Gaussian processes and $\tilde{S}_j(\omega) = \partial S_s(\omega)/\partial a_j$ exists for $1 \leq j \leq n$. Denoting $\boldsymbol{\psi} = [\theta, \phi, \mathbf{a}^T]^T$, we compute the CRB on the $n+2$ unknown parameters as follows:

$$\mathbf{CRB}(\boldsymbol{\psi}) = \begin{bmatrix} J_{\theta\theta} & J_{\theta\phi} & \boldsymbol{J}_{\theta\mathbf{a}} \\ J_{\theta\phi}^* & J_{\phi\phi} & \boldsymbol{J}_{\phi\mathbf{a}} \\ \boldsymbol{J}_{\theta\mathbf{a}}^* & \boldsymbol{J}_{\phi\mathbf{a}}^* & \mathbf{J}_{\mathbf{aa}} \end{bmatrix}^{-1} \tag{7}$$

where [see (8)–(12) at the bottom of the next page].

See the Appendix for detailed derivations.

$$\mathbf{J}(\boldsymbol{\psi})_{kl} = \frac{N}{4\pi}\int_{-\pi}^{\pi} \mathrm{tr}\left\{\frac{\partial \mathbf{S}_y(\omega,\boldsymbol{\psi})}{\partial\psi_k}\,\mathbf{S}_y^{-1}(\omega,\boldsymbol{\psi})\,\frac{\partial \mathbf{S}_y(\omega,\boldsymbol{\psi})}{\partial\psi_l}\,\mathbf{S}_y^{-1}(\omega,\boldsymbol{\psi})\right\} d\omega, \quad 1 \leq k,\, l \leq M \tag{6}$$

IV. Numerical Results

To illustrate the analytical results on the accuracy of target-direction and source parameter estimation, we evaluated the CRB (7) for a variety of scenarios. For all the results presented in this section, we considered the following:

- reflection coefficients of both the reflectors $\rho_z = \rho_y = 1$;
- distance of the reflector parallel to XY plane from the sensor $z_{\mathrm{r}} = 2$ m;
- distance of the reflector parallel to XZ plane from the sensor $y_{\mathrm{r}} = 3$ m;
- speed of light $c = 3 \times 10^8$ m/s;
- sampling frequency $f_s = 200$ MHz.

The power spectral density of the noise process is assumed to be flat over the whole frequency range $[-\pi, \pi]$. We consider the source signal as a second-order AR process modeled as

$$S_s(\omega) = \frac{1}{(1 + a_1^2 + a_2^2) - 2a_1(1 + a_2^2)\cos\,\omega + 2a_2 \cos\,2\omega}. \quad (13)$$

This model was obtained by considering a conjugate pole-pair at $de^{\pm j\omega_0}$ and denoting $a_1 = 2d\cos\,\omega_0$ and $a_2 = d^2$. We denote ω_{cf} as the central frequency and ω_{bw} as the 3-dB bandwidth of the source spectrum. In the subsequent results, we consider the signal-to-noise ratio (SNR) as $\mathrm{SNR} = \left[\int_{-\pi}^{\pi} S_s(\omega)d\omega\right] / (2\pi S_e)$ and the normalized bandwidth as $B = \omega_{\mathrm{bw}}/\pi$. We present our results in the following three subsections.

A. CRB Variations With Respect to SNR

Fig. 3(a) depicts the square-root of the Cramér–Rao bound on the elevation angle estimation as a function of SNR. Fig. 3(b) represents the same type of result for the azimuth angle estimation. As expected, the CRB decreases as SNR is increased. In Fig. 4, we plot the square-root of the CRB on estimated bandwidth and central frequency of the source spectrum as a function of SNR. These can be obtained from the CRB matrix of a_1 and a_2 using the following relation:

$$\mathbf{CRB}(\boldsymbol{\nu}) = \frac{\partial \boldsymbol{g}(\boldsymbol{\eta})}{\partial \boldsymbol{\eta}} \mathbf{CRB}(\boldsymbol{\eta}) \frac{\partial \boldsymbol{g}^T(\boldsymbol{\eta})}{\partial \boldsymbol{\eta}} \quad (14)$$

where $\boldsymbol{\nu} = \boldsymbol{g}(\boldsymbol{\eta})$ is the relationship between $\boldsymbol{\nu} = [\omega_{\mathrm{bw}}\ \omega_{\mathrm{cf}}]^T$ and $\boldsymbol{\eta} = [a_1\ a_2]^T$. For this example, we kept the true values of the parameters as $\theta = 30^\circ$, $\phi = 30^\circ$, and $a_1 = 0.59$, $a_2 = 0.9$ which corresponds to a conjugate pole-pair at $0.95e^{\pm j0.4\pi}$. These results were obtained with $N = 5000$.

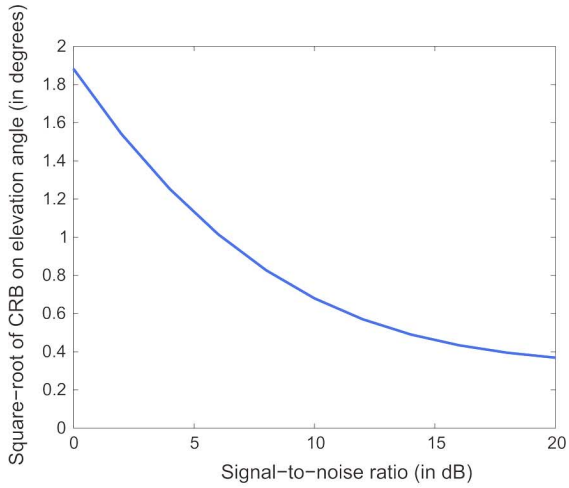

Fig. 3. Square-root of the Cramér–Rao bound on estimated (a) elevation angle and (b) azimuth angle as a function of SNR for two nearby reflectors.

B. CRB Variations With Respect to Normalized Bandwidth

Fig. 5 shows the variation of the square-root of the CRB on the estimated elevation and azimuth angles as a function of normalized bandwidth (B) for a fixed value of $\mathrm{SNR} = 5$ dB. From these results, we observe that for a wider source spectrum we can efficiently resolve

$$J_{\theta\phi} = \frac{N}{2\pi}\int_{-\pi}^{\pi}\left[\left(\frac{S_s}{S_{\mathrm{T}}}\right)^2 \mathrm{Re}\left\{\frac{\partial H^*}{\partial\theta} H \frac{\partial H^*}{\partial\phi} H\right\} + \left(\frac{|H|^2 S_s^2}{S_{\mathrm{T}}}\right) \mathrm{Re}\left\{\frac{\partial H^*}{\partial\theta} S_y^{-1} \frac{\partial H}{\partial\phi}\right\}\right] d\omega \quad (8)$$

$$J_{\theta a_j} = \frac{N}{2\pi}\int_{-\pi}^{\pi} \tilde{S}_j \left(\frac{|H|^2 S_s}{S_{\mathrm{T}}^2}\right) \mathrm{Re}\left\{\frac{\partial H^*}{\partial\theta} H\right\} d\omega \quad \text{for } 1 \le j \le n \quad (9)$$

$$J_{\phi a_j} = \frac{N}{2\pi}\int_{-\pi}^{\pi} \tilde{S}_j \left(\frac{|H|^2 S_s}{S_{\mathrm{T}}^2}\right) \mathrm{Re}\left\{\frac{\partial H^*}{\partial\phi} H\right\} d\omega \quad \text{for } 1 \le j \le n \quad (10)$$

$$J_{a_i a_j} = \frac{N}{4\pi}\int_{-\pi}^{\pi} \tilde{S}_i \tilde{S}_j \left(\frac{|H|^2}{S_{\mathrm{T}}}\right)^2 d\omega \quad \text{for } 1 \le i, j \le n \quad (11)$$

$$S_{\mathrm{T}} = S_e + |H|^2 S_s. \quad (12)$$

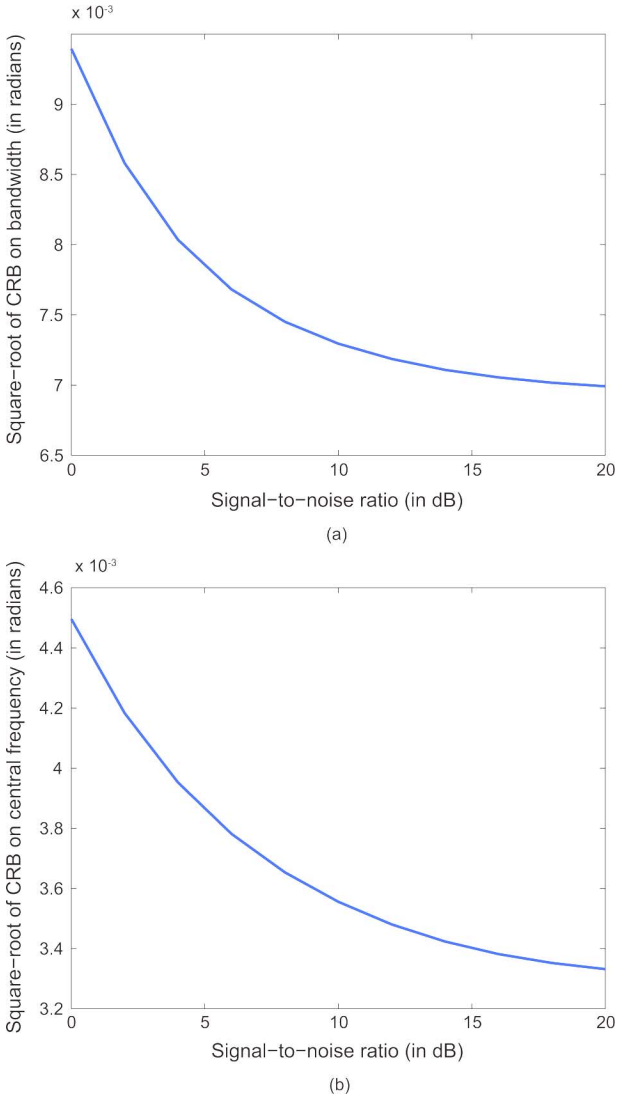

Fig. 4. Square-root of the Cramér–Rao bound on (a) bandwidth and (b) central frequency estimations of the source spectrum as a function of SNR for two nearby reflectors.

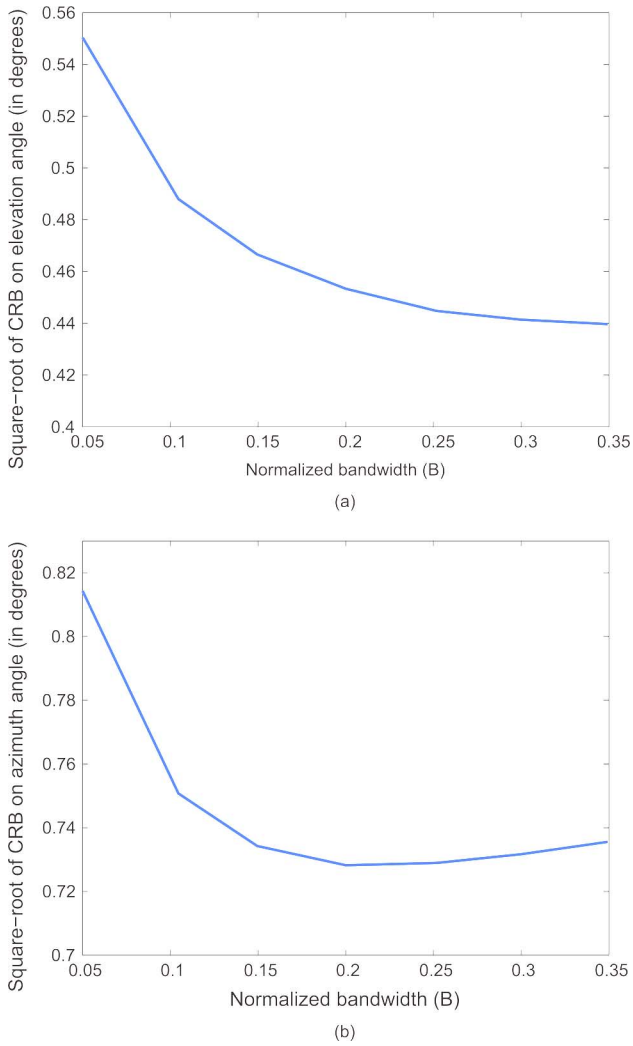

Fig. 5. Square-root of the Cramér–Rao bound on (a) elevation angle and (b) azimuth angle estimations as a function of normalized bandwidth of the source spectrum for two nearby reflectors.

the close-range multipath reflections and achieve better direction estimates. As before, we fixed the true values of the parameters as $\theta = 30^\circ$ and $\phi = 30^\circ$. These results were also simulated with $N = 5000$.

C. CRB Variations After Adding One More Reflector

We modified our model, depicted in Fig. 2, by adding one more reflector parallel to the YZ plane at a distance x_{r} from the source, as shown in Fig. 6. We proceed with a similar type of analysis and obtain the CRB on the directional angles and the source parameters for a zero-mean wide-sense stationary Gaussian source signal modeled as a second-order AR process. We simulate this scenario for $\rho_x = 1$ and $x_{\mathrm{r}} = 3$ m, keeping all the other parameters as before. Fig. 7 illustrates the variation of the square-root of the CRB on the elevation and azimuth angles as a function of SNR. Fig. 8 represents the same type of results for the estimated bandwidth and central frequency of the source spectrum. For comparison, in the same figures we also include the results obtained with two nearby reflectors, which implies that by applying additional reflectors we can obtain better estimates of the target-direction.

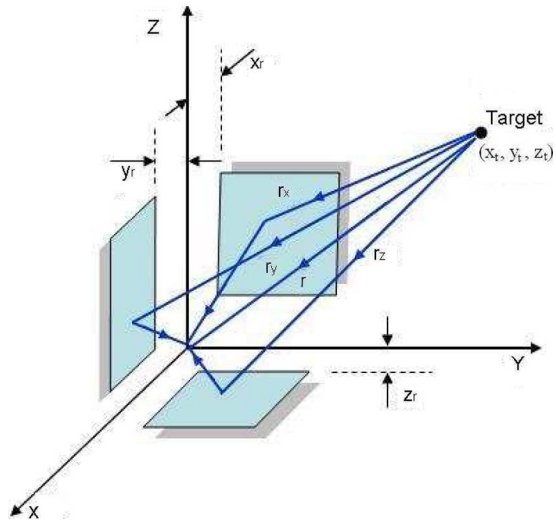

Fig. 6. Multipath reflections close to the sensor with three nearby reflectors.

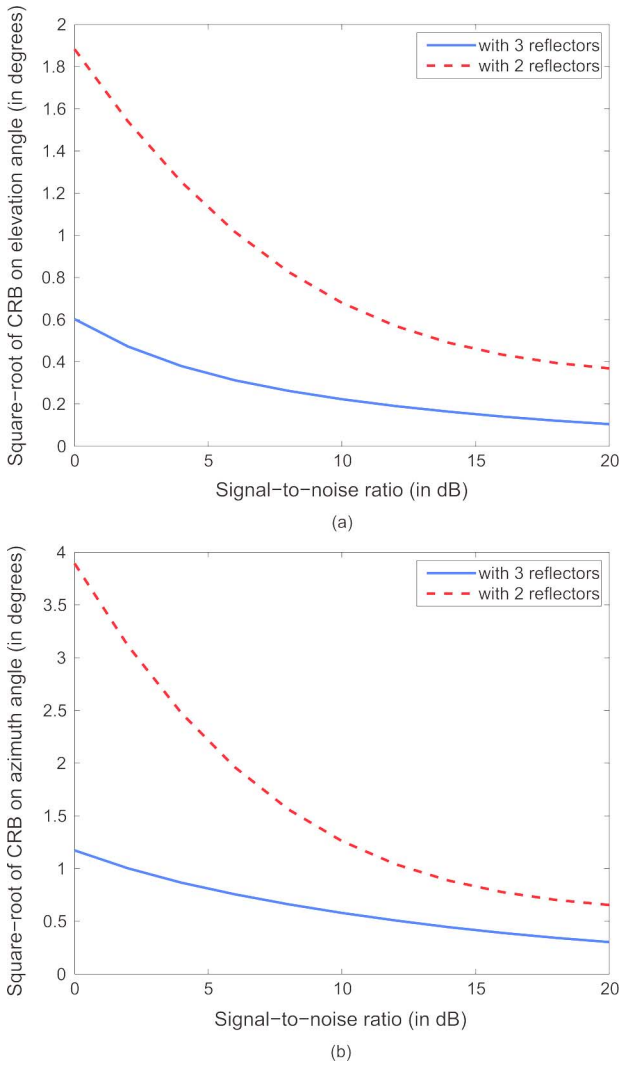

Fig. 7. Square-root of the Cramér–Rao bound on estimated (a) elevation angle and (b) azimuth angle as a function of SNR for two and three nearby reflectors.

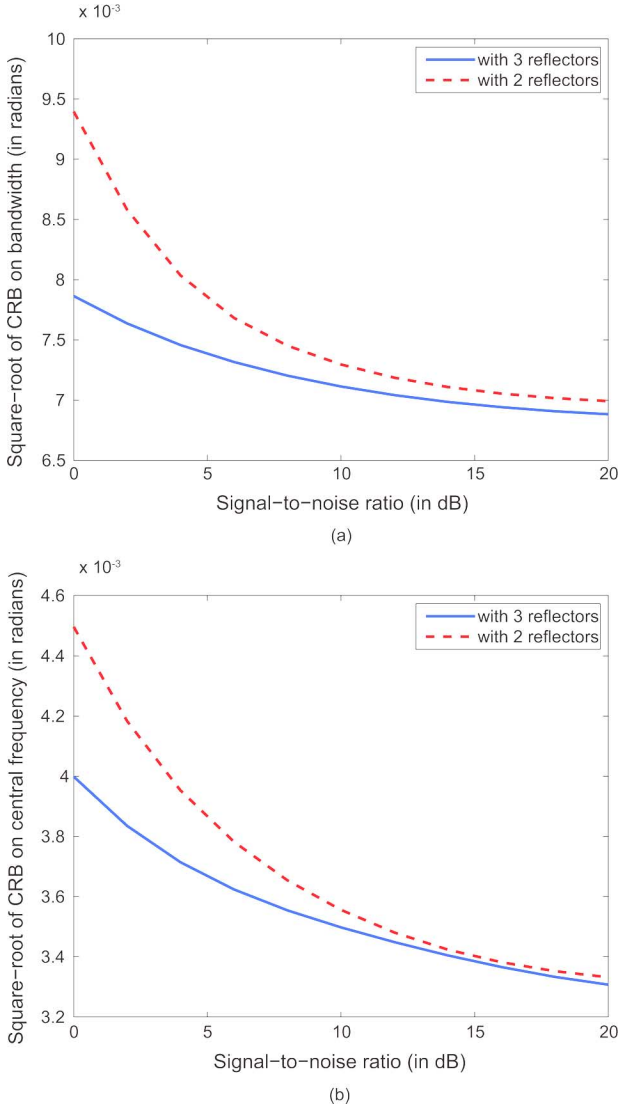

Fig. 8. Square-root of the Cramér–Rao bound on estimated (a) bandwidth and (b) central frequency of the source spectrum as a function of SNR for two and three nearby reflectors.

V. Conclusion

We have proposed that by exploiting multipath reflections close to the sensor we can improve the 3-D direction estimation of a target. To demonstrate this advantage, we consider a simple example of a passive system with only one sensor and two nearby reflectors. This model can be easily extended to a more complicated system having more reflectors. Our approach is inspired by the pinna multipath reflections of the human hearing system. We analyze the performance of our model by computing the Cramér–Rao bound on the direction estimate for wideband stochastic Gaussian source signals of an unknown parametrized spectrum. Our numerical results imply that location accuracy improves when multiple reflectors are employed and a wider source spectrum is used. In our future work, we will analyze the identifiability of our model in terms of the number of sensors and reflectors. We will also incorporate more practical aspects, such as random multipath reflections. For a given sensor platform, we will optimize the positioning of the reflectors to maximize system performance for realistic scenarios.

Appendix

In this section, we demonstrate the steps for computing the expression of $J_{\theta\phi}$, $J_{\theta a_j}$, and $J_{a_i a_j}$. The other entries of the FIM can be obtained following a similar procedure. We know that

$$\frac{\partial S_y}{\partial \theta} = \frac{\partial H}{\partial \theta} S_s H^* + H S_s \frac{\partial H^*}{\partial \theta} \tag{A-1}$$

$$\frac{\partial S_y}{\partial \phi} = \frac{\partial H}{\partial \phi} S_s H^* + H S_s \frac{\partial H^*}{\partial \phi} \tag{A-2}$$

$$\frac{\partial S_y}{\partial a_j} = \frac{\partial S_s}{\partial a_j}|H|^2 = \tilde{S}_j |H|^2 \quad \text{for } 1 \le j \le n. \tag{A-3}$$

Further, using Woodbury's matrix inversion identity in (5), we have

$$S_y^{-1} = \left(\frac{1}{S_e}\right)\left[1 - H\left(\frac{S_e}{S_s} + |H|^2\right)^{-1} H^*\right]. \tag{A-4}$$

Using (A-1)–(A-4), after some algebraic manipulation we get

$$\frac{\partial S_y}{\partial \theta} S_y^{-1} = \frac{\partial H}{\partial \theta}\left(\frac{S_e}{S_s} + |H|^2\right)^{-1} H^* + H S_s \frac{\partial H^*}{\partial \theta} S_y^{-1} \tag{A-5}$$

$$\begin{aligned}
\mathrm{tr}\left\{\frac{\partial S_y}{\partial\theta}\,S_y^{-1}\,\frac{\partial S_y}{\partial\theta}\,S_y^{-1}\right\} &= \left(\frac{S_s}{S_{\mathrm{T}}}\right)^2 H^*\,\frac{\partial H}{\partial\theta}H^*\,\frac{\partial H}{\partial\theta} + \left(\frac{S_s^2}{S_{\mathrm{T}}}\right)|H|^2\,\frac{\partial H^*}{\partial\theta}S_y^{-1}\frac{\partial H}{\partial\theta} \\
&\quad + \left(\frac{S_s^2}{S_{\mathrm{T}}}\right)|H|^2\frac{\partial H^*}{\partial\theta}S_y^{-1}\frac{\partial H}{\partial\theta} \\
&\quad + \left(\frac{S_s}{S_{\mathrm{T}}}\right)^2\frac{\partial H^*}{\partial\theta}H\frac{\partial H^*}{\partial\theta}H = 2\,\left(\frac{S_s}{S_{\mathrm{T}}}\right)^2\mathrm{Re}\left\{\frac{\partial H^*}{\partial\theta}H\frac{\partial H^*}{\partial\theta}H\right\} \\
&\quad + 2\,\left(\frac{S_s^2}{S_{\mathrm{T}}}\right)|H|^2\,\mathrm{Re}\left\{\frac{\partial H^*}{\partial\theta}S_y^{-1}\frac{\partial H}{\partial\theta}\right\} \\
\mathrm{tr}\left\{\frac{\partial S_y}{\partial\theta}\,S_y^{-1}\,\frac{\partial S_y}{\partial a_j}\,S_y^{-1}\right\} &= \tilde{S}_j\left(\frac{S_s}{S_{\mathrm{T}}}\right)|H|^2\left\{H^*S_y^{-1}\frac{\partial H}{\partial\theta}\right\} + \tilde{S}_j\left(\frac{S_s}{S_{\mathrm{T}}}\right)|H|^2\left\{\frac{\partial H^*}{\partial\theta}S_y^{-1}H\right\} \\
&= 2\tilde{S}_j\left(\frac{S_s}{S_{\mathrm{T}}^2}\right)|H|^2\,\mathrm{Re}\left\{\frac{\partial H^*}{\partial\theta}H\right\} \\
\mathrm{tr}\left\{\frac{\partial S_y}{\partial a_i}\,S_y^{-1}\,\frac{\partial S_y}{\partial a_j}\,S_y^{-1}\right\} &= \tilde{S}_i\tilde{S}_jH^*S_y^{-1}|H|^2S_y^{-1}H = \tilde{S}_i\tilde{S}_j\left(\frac{|H|^2}{S_{\mathrm{T}}}\right)^2.
\end{aligned}$$

$$\frac{\partial S_y}{\partial a_j}\,S_y^{-1} = \tilde{S}_j|H|^2\,S_y^{-1}. \tag{A-6}$$

Therefore

$$\begin{aligned}
\frac{\partial S_y}{\partial\theta}\,S_y^{-1}\,\frac{\partial S_y}{\partial\phi}\,S_y^{-1} &= \frac{\partial H}{\partial\theta}\left(\frac{S_e}{S_s}+|H|^2\right)^{-1}H^* \\
&\quad\cdot\frac{\partial H}{\partial\phi}\left(\frac{S_e}{S_s}+|H|^2\right)^{-1}H^* \\
&\quad+\frac{\partial H}{\partial\theta}\left(\frac{S_e}{S_s}+|H|^2\right)^{-1}|H|^2\,S_s\,\frac{\partial H^*}{\partial\phi}S_y^{-1} \\
&\quad+H\,S_s\,\frac{\partial H^*}{\partial\theta}S_y^{-1}\,\frac{\partial H}{\partial\phi}\left(\frac{S_e}{S_s}+|H|^2\right)^{-1}\,H^* \\
&\quad+H\,S_s\,\frac{\partial H^*}{\partial\theta}S_y^{-1}H\,S_s\,\frac{\partial H^*}{\partial\phi}S_y^{-1} \\
\frac{\partial S_y}{\partial\theta}\,S_y^{-1}\frac{\partial S_y}{\partial a_j}\,S_y^{-1} &= \tilde{S}_j\frac{\partial H}{\partial\theta}\left(\frac{S_e}{S_s}+|H|^2\right)^{-1}|H|^2H^*S_y^{-1} \\
&\quad+\tilde{S}_jHS_s\frac{\partial H^*}{\partial\theta}S_y^{-1}|H|^2S_y^{-1} \\
\frac{\partial S_y}{\partial a_i}\,S_y^{-1}\frac{\partial S_y}{\partial a_j}\,S_y^{-1} &= \tilde{S}_i\tilde{S}_j|H|^2\,S_y^{-1}|H|^2\,S_y^{-1}.
\end{aligned}$$

From (12), we get $\left(S_e/S_s+|H|^2\right)^{-1} = S_s/S_{\mathrm{T}}$ and $S_y^{-1}H = H/S_{\mathrm{T}}$. Then, using the properties of the trace operator, we get the equation shown at the top of the page. Substituting these into (6), we obtain the expressions given in (8)–(11).

REFERENCES

[1] D. W. Batteau, "The role of the pinna in human localization," *Proc. Royal Soc. London, Series B, Biolog. Sci.*, vol. 168, no. 1011, Aug. 1967.

[2] S. K. Roffler and R. A. Butler, "Factors that influence the localization of sound in the vertical plane," *J. Acoust. Soc. Amer.*, vol. 43, no. 6, pp. 1255–1259, Jun. 1968.

[3] S. R. Oldfield and S. P. A. Parker, "Acuity of sound localisation: A topography of auditory space. II. Pinna cues absent," *Perception*, vol. 13, no. 5, pp. 601–617, 1984.

[4] P. M. Hofman, J. G. A. V. Riswick, and A. J. V. Opstal, "Relearning sound localization with new ears," *Nature Neurosci.*, vol. 1, no. 5, pp. 417–421, Sep. 1998.

[5] C. P. Brown and R. O. Duda, "A structural model for binaural sound synthesis," *IEEE Trans. Speech Audio Process.*, vol. 6, no. 5, pp. 476–488, Sep. 1998.

[6] J. G. Harris, C.-J. Pu, and J. C. Principe, "A neuromorphic monaural sound localizer," in *Proc. 1998 Conf. Adv. Neural Inf. Process. Syst.*, Cambridge, MA, 1998, pp. 692–698.

[7] S. Sen and A. Nehorai, "Performance analysis of 3-D direction estimation based on head-related transfer function," *IEEE Trans. Audio, Speech, Lang. Process.*, unpublished.

[8] P. Whittle, "The analysis of multiple stationary time series," *J. Royal Statist. Soc., Series B (Methodolog.)*, vol. 15, no. 1, pp. 125–139, 1953.

[9] S. M. Kay, *Fundamentals of Statistical Signal Processing: Estimation Theory*. Upper Saddle River, NJ: Prentice-Hall PTR, 1993.

[10] A. Zeira and A. Nehorai, "Frequency domain Cramér-Rao bound for Gaussian processes," *IEEE Trans. Acoust., Speech, Signal Process.*, vol. 38, no. 6, pp. 1063–1066, Jun. 1990.

[11] C. P. Brown, "Modeling the elevation characteristics of the head-related impulse response," Master's thesis, San Jose State Univ., San Jose, CA, May 1996.